BNL-212113-2019-JAAM

Inhomogeneous structural evolution of silver-containing Alpha-MnO2 nanorods in sodium-ion batteries investigated by comparative transmission electron microscopy approach

S. Lee, Y. Zhu

To be published in "JOURNAL OF POWER SOURCES"

September 2019

Condensed Matter Physics and Materials Science Department

Brookhaven National Laboratory

U.S. Department of Energy

USDOE Office of Science (SC), Basic Energy Sciences (BES) (SC-22)

DISCLAIMER

Inhomogeneous Structural Evolution of Silver-Containing alpha-MnO_2 Nanorods in Sodium-Ion Batteries Investigated by Statistical Transmission Electron Microscopy Approach

Seung-Yong Lee, Jianping Huang, Lisa M. Housel, Lijun Wu, Esther S. Takeuchi, Amy C. Marschilok, Kenneth J. Takeuchi, Miyoung Kim*, and Yimei Zhu**

Dr. S.-Y. Lee, Dr. L. Wu, Prof. Y. Zhu
Condensed Matter Physics and Materials Science Department, Brookhaven National Laboratory, Upton, New York 11973, USA.
e-mail: zhu@bnl.gov

Dr. S.-Y. Lee, Prof. M. Kim
Department of Materials Science and Engineering and Research Institute of Advanced Materials, Seoul National University, Seoul 08826, Republic of Korea.
e-mail: mkim@snu.ac.kr

Mr. J. Huang, Ms. Lisa M. Housel, Prof. A. C. Marschilok, Prof. K. J. Takeuchi, Prof. E. S. Takeuchi
Department of Chemistry and Department of Materials Science and Engineering, Stony Brook University, Stony Brook, New York 11794, USA.
e-mail: kenneth.takeuchi.1@stonybrook.edu

Prof. A. C. Marschilok, Prof. E. S. Takeuchi
Energy Sciences Directorate, Brookhaven National Laboratory, Upton, New York 11973, USA.

Keywords: sodium ion battery, manganese oxide, transmission electron microscopy, electrochemical reaction mechanism.

Abstract

Alpha-MnO_2 is an attractive cathode candidate for sodium-ion batteries attributed to its unique one-dimensional 2 × 2 tunnels providing efficient channels for facile sodium-ion diffusion, in addition to its incomparable cost advantage. In particular, α-MnO_2 shows superior rate capability with silver stabilizing ions at the center of tunnels by developing silver metal nanoprecipitates on the materials during sodiation that improve electrical conductivity. However, the silver-containing α-MnO_2 shows performance drop with excessive density of silver ions accompanied by less oxygen vacancies, which demands fundamental investigation on the structural evolution of α-MnO_2 cathode in sodium-ion batteries. In this work, we directly compare structural transformation of silver-containing α-MnO_2 nanorods ($Ag_{1.22}Mn_8O_{16}$ and $Ag_{1.66}Mn_8O_{16}$), containing high and low concentration of oxygen vacancies respectively, by stastical transmission electron microscopy (TEM) approaches. The elaborate statistical TEM studies eliminate concerns on the generalization error and facilitate examination of variations in structural development among nanorods. We reveal that excessive silver ions and a few oxygen vacancies in α-MnO_2 nanorods accelerate structural deformation with severe inhomogeneity all over the material. It is found that sodium ions favorably diffuse through the area where oxygen vacancies are concentrated. The inter- and intra-nanorod inhomogeneous structural evolution emphasizes the importance of the uniform electrical conductivity of the electrode. This work helps to elucidate possible directions for improvement of the attractive α-MnO_2 electrode material for sodium-ion batteries as well as providing delicate statistical approaches for TEM investigations.

Taking advantages of high energy densities, lithium-ion batteries have been extensively used for energy-storage applications, however, the high cost of lithium resources has led to the investigation of alternatives for large-scale applications. Sodium-ion batteries are attracting great attention as a promising alternative due to the abundance of sodium in the Earth.[1] The operating principle which is analogous to lithium-ion batteries has contributed to their rapid development. However, the differences on physical properties between lithium and sodium ions, e.g. reduction potential, ionic size, diffusivity, and etc., drive researchers to find novel materials suited for sodium-ion batteries and to investigate their own reaction behaviors.[1-3]

Having one-dimensional 2 × 2 tunnels, hollandite-type alpha-phase manganese dioxide (α-MnO_2) is an attractive candidate for various rechargeable metal-ion battery cathodes including sodium-ion batteries.[4-8] It is known that the tunnels, spacious enough to accommodate several sodium ions without structural collapse, are beneficial for facile cation diffusion by an insertion reaction in the conventional voltage range of sodium-ion battery cathodes.[4-5] In nature, α-MnO_2 minerals contain foreign cations, such as K^+ or Ba^{2+}, at the center of the wide 2 × 2 tunnels to stabilize the tunnel structure.[9-10] Inspired by the nature, α-MnO_2 materials have been typically synthesized with a stabilizer at the center of tunnels, e.g. K^+, Ag^+, Li_2O, NH_3, or H_2O.[10-12] In particular, we recently showed that silver-containing α-MnO_2 materials can deliver superior performance for a sodium-ion battery cathode attributed to the additional positive influence of silver stabilizing ions.[5] In our previous study, it was found that several silver ions extruded from the tunnels during sodium-ion insertion (sodiation) form silver metal nano-precipitates onto the surface of the silver-containing α-MnO_2 nanorods, which improve rate capability of the cathode by increasing electrical conductivity of the nanorods.[5, 13] However, α-MnO_2 nanorods containing excessive silver ions concurrent with less oxygen vancacies showed worse performance, which complicates further development of the material. It was predicted that low concentration of oxygen vacancies may have hindered facile sodium-ion diffusion

across the tunnels,[5, 14] but it still remains unknown how the tunnel structure is influenced and deteriorated by those significant factors during sodiation.

In this study, we directly compared the structural evolution of $Ag_{1.22}Mn_8O_{16}$ (L-Ag-HOL) and $Ag_{1.66}Mn_8O_{16}$ (H-Ag-HOL) nanorods, containing high and low concentration of oxygen vacancies respectively, under various sodiation levels by statistical transmission electron microscopy (TEM) approaches. The statistical approaches on high-resolution TEM (HRTEM) and electron energy loss spectroscopy (EELS) analyses facilitated macro- and micro-scopic structural investigation simultaneously, which eliminated the possibility of the generalization error and maximized the advantage on nano-investigation of TEM. By this comprehensive TEM study, we found that fewer oxygen vacancies and higher Ag-ion concentration accelerate overall structural evolution of MnO_2 at lower sodiation levels, completing conversion reaction of α-MnO_2 into MnO phase at earlier sodiation stage. More importantly, it was revealed that higher resistance for sodium-ion diffusion in α-MnO_2 nanorods caused by less oxygen vacancies and more Ag-ion concentration induces severe inhomogeneous structural evolution in the whole electrode, including inter- and intra-nanorods, which is an important factor that hinders electrodes from showing their best performance.[15-16] This study provides further understanding on sodiation behaviors of silver-containing α-MnO_2 materials depending on the concentration of silver ions and oxygen vacancies, which is expected shed insight into the future development of the attractive α-MnO_2 sodium-ion battery cathode. In addition, our experimental results emphasize the importance of statistical approaches on TEM studies, vulnerable to the generalization error.

An atomic structural model of silver-containing α-MnO_2 nanorods is shown in Figure 1a, whereeight MnO_6 octahedra form the 2×2 tunnels. It is known that these tunnels greatly contribute to facile cation diffusion in α-MnO_2 electrodes for metal-ion batteries, which make α-MnO_2 materials attractive in the field of secondary batteries.[4-8] As shown in the model, silver

ions occupy center of the tunnels, stabilizing this structure. Up to two silver ions can occupy this site per unit cell, Mn_8O_{16}. Silver-ion concentrations of L-Ag-Hol ($Ag_{1.22}Mn_8O_{16}$) and H-Ag-Hol ($Ag_{1.66}Mn_8O_{16}$) materials were determined by inductively coupled plasma optical emission spectroscopy (ICP-OES).

Figure 1b–f show representative HRTEM images and corresponding fast Fourier-transformed (FFT) patterns of H-Ag-HOL nanorods with different sodiation levels. Sodium ions were electrochemically inserted into the nanorods in coin-type $Na/Ag_{1.66}Mn_8O_{16}$ half cells.[5] The voltage profiles for sodiation of L-Ag-Hol and H-Ag-HOL under rates of 20 mA/g (Figure S2a) or 2 mA/g (Figure S2b) of active material are provided. Under the 20 mA/g rate, the kinetic limitation for H-Ag-HOL is apparent as less than 1 molar equivalent of sodiation was achieved. However, under the lower current of 2 mA/g as used for the samples for analysis, both materials effectively sodiate to greater than 8 molar equivlents. Pristine H-Ag-HOL nanorods have flat surfaces as shown in Figure 1b. After sodium ions were inserted, tiny particles are created at the surface of the H-Ag-HOL nanorods (Figure 1c). The particles are clearly visible in high-angle annular dark-field (HAADF) scanning TEM (STEM) images and they were identified as silver metal (Figure S1). The silver particles have also been observed on the sodiated L-Ag-HOL nanorods as already shown in our previous paper.[5] It implies that sodium ions compete with silver ions in the tunnels during sodiation and displace silver ions from the tunnels. Silver precipitates tend to become bigger with high sodiation levels as shown in Figure 1c–f. It may be attributed to the extrusion and aggregation of more silver ions with higher concentration of sodium ions in the tunnels. Despite this structural change that may be irreversible, the silver precipitates on the surface of nanorods are of help to the performance of hollandite SIB electrode up to specific amount, by improving electrical conductivity.[5]

FFT patterns in the insets of Figure 1b–f show apparent crystal structural transformation after 6 Na ions inserted into the unit cell of H-Ag-HOL, i.e. $Ag_{1.66}Mn_8O_{16}$. Up

to 4 Na ions are inserted in the nanorods, streaks are aligned in the FFT patterns perpendicular to the longitudinal direction of tunnels (Figure 1b–d). The streaks originate from defects of tunnel structure that create numerous unexpected diffraction peaks, however, the presence of the streaks analogous to the pristine nanorods imply that the tunnel framework is mostly well preserved up to 4 Na ions in $Ag_{1.66}Mn_8O_{16}$. From 6 Na ions in the unit cell, the shape is apparently changed and streaks disappeared in the FFT patterns, which indicate noticeable structural transformation at this stage. We found that the FFT patterns in Figure 1e and f correspond to MnO structure with preferred orientation evolved from α-MnO_2 material by conversion reaction mechanism.[17]

The structural evolution of Ag-HOL materials can be further understood with Figure 2. It directly compares averaged radial intensity profiles of FFT patterns obtained from HRTEM images of pristine/sodiated L-Ag-HOL and H-Ag-HOL nanorods up to 8 Na-ion levels. Each curve is the sum of normalized radial intensity profiles acquired from over 15 different HRTEM-FFT patterns. Each HRTEM image included several nanowires. Accordingly, these statistically processed data clearly describe overall structural evolution of the materials with sufficient representativeness, which TEM data are often vulnerable to. In Figure 2, radial intensity profiles at large interplanar spacing range (over 0.4 nm) are not plotted to avoid potential unwanted influence of FFT on the rings from an amorphous carbon supporting film on a TEM grid. As shown in the figure, both materials transform their structure from MnO_2 to MnO during sodiation, but L-Ag-HOL and H-Ag-HOL show slightly different sodiaton behaviors. In L-Ag-HOL nanorods (Figure 2a), FFT peaks originating from the MnO structural feature begin to appear from 2 Na-ion level. There is a slight strain-induced mismatch of interplanar spacing with that of ideal MnO phase. As L-Ag-HOL is further sodiated, FFT peak positions gradually move to the interplanar spacing of ideal MnO lattice planes, which is apparent in MnO {002} peaks. It indicates gradual structural transformation and strain

relaxation with increasing sodiation levels. However, the structure still deviates from the perfect MnO until 8 Na-ion levels.

In H-Ag-HOL (Figure 2b), it shows broad FFT peaks between the interplanar spacing range of 0.24 nm to 0.3 nm up to 4 Na-ion levels. It is attributed to the co-existence of MnO_2 and MnO structure at these sodiation levels, which implies the inhomogeneous structural evolution among respective nanorods or intra-nanorod. Compared to L-Ag-HOL nanorods at these sodiation levels, the inhomogeneous sodiation is obvious in H-Ag-HOL nanorods that undergo higher resistance during sodiation by containing more silver ions that compete with sodium ions and less oxygen vancancies that ease sodium-ion diffusion.[5, 14] From 6 Na-ion level, the MnO structural feature is clearly observed in the FFT intensity profile of the H-Ag-HOL sample (Figure 2b), which coincides with the HRTEM-FFT patterns shown in Figure 1. Furthermore, the FFT peak positions well match with ideal MnO stucture at 8 Na-ion level in H-Ag-HOL, much better than L-Ag-HOL, which indicates that most of α-MnO_2 nanorods are transformed into typical MnO structure without strain at this sodiation stage of H-Ag-HOL, earlier than L-Ag-HOL. It also implies that the insertion reaction, accommodating Na ions in the tunnel structure, is limited to lower sodiation levels in H-Ag-HOL compared to L-Ag-HOL; this agrees well with higher charge transfer resistance of H-Ag-HOL than L-Ag-HOL measured and shown in our previous research.[5] Insert comment about new echem here and add figure in SI.

Figure 3 clearly shows serious inhomogeneity of sodiation in H-Ag-HOL. It shows Mn L_3/L_2-edge intensity ratios of experimental electron energy loss spectroscopy (EELS) data acquired from pristine/sodiated L-Ag-HOL and H-Ag-HOL samples, which were measured in TEM-diffraction mode. Given that this result reflects the oxidation state of manganese ions, the Mn L_3/L_2-edge intensity ratio is an excellent indicator to estimate structural evolution of MnO_2 by sodiation.[17, 19-21] For the statistical approach, TEM-EELS data was obtained from over

20 different regions per each sample and each region contains several nanowires. The Mn L_3/L_2-edge intensity ratio was calculated based on Pearson method with double step functions.[18] Mn L_3- and L_2-edge intensities were measured by integrating intensities of 4 eV width range centered at the peak maximum. All measured Mn L_3/L_2-edge intensity ratio values from TEM-EELS data are drawn with open circles. Average and standard deviation from each sample are also plotted with a column and an error bar.

Manganese oxides show higher Mn L_3/L_2-edge intensity ratios with lower oxidation states between the range of Mn^{2+} (MnO) and Mn^{4+} (MnO_2).[17, 19-21] Accordingly, Mn L_3/L_2-edge intensity ratio of hollandite structured MnO_2 (α-MnO_2) will increase with higher Na-ion concentration at the early sodiation stages that transforms MnO_2 into $Na_xMn_8O_{16}$ by insertion reaction and MnO by conversion reaction. As expected, the average of Mn L_3/L_2-edge intensity ratios increase with higher sodiation levels from 0 to 8 Na-ion per Mn_8O_{16} unit structure in both of L-Ag-HOL and H-Ag-HOL samples (Figure 3). However, there are slight differences observed bewteen the two samples. Given the contribution of silver ions to the electroneutrality, H-Ag-HOL, containing more silver ions, is expected to have lower oxidation state of manganese ions than L-Ag-HOL in the pristine state, which should result in higher Mn L_3/L_2-edge intensity ratio. However, it shows the opposite result on average, which demonstrates the higher concentration of oxygen vacancies in L-Ag-HOL nanorods that contributes to the increment of Mn oxidation state.[14] As soon as the nanorods are sodiated, H-Ag-HOL shows higher average Mn L_3/L_2-edge intensity ratio than L-Ag-HOL. It implies that H-Ag-HOL nanorods undergo greater structural transformation at the same sodiation levels, which may be attributed to their higher resistance hindering facile sodiation and breaking the tunnel structure easier. In addition, the H-Ag-HOL sample shows larger deviation of structural evolution among nanorods than L-Ag-HOL at every sodiation levels. The larger deviation is easily recognized by the distribution of Mn L_3/L_2-edge intensity ratios from each TEM-EELS data indicated with

open circles in Figure 3. It indicates that the sodiation into silver hollandite is greatly affected by Ag-ion concentration and oxygen vacancies, both of which result in severe inhomogeneous sodiation of silver hollandite depending on local Ag-ion and oxygen vancancy concentrations of the nanorods. In particular, the deviation of Mn L_3/L_2-edge intensity ratios tends to increase with higher sodiation levels in H-Ag-HOL, which is remarkable at the 8 Na-ion level. These data confirm the significant influence of local environment into smooth Na-ion diffusion.

Figure 4 demonstrates the inhomogeneous structural evolution in H-Ag-HOL. The figure shows representative HRTEM images of H-Ag-HOL nanorods sodiated up to a 8 Na-ion level. Yellow dashed curves indicate the regions where the hollandite crystalline structure transformed into an amorphous structure. The amorphization implies severe structural deformation and collapse from its original structure, which may have occurred by excessive concentration of sodium ions. As shown in the HRTEM images, the amorphized regions are scattered over the nanorods, but are more frequently near the surface where oxygen vacancies are concentrated.[14] On the other hand, the tunnel structure is still maintained in several regions at the core of nanorods. The structural difference is clearly compared by FFT patterns in Figure 4c and d. Vertical streaks originating from tunnels are observed in the FFT pattern obtained from the core of the nanorod indicated as Region (i) (Figure 4c), however, only a few broken peaks are shown from Region (ii) near the surface (Figure 4d). Therefore, it shows that inhomogeneous structural evolution can be intensified even in a single nanorod can be deeply influenced by oxygen vacancy concentration that eases sodium ion diffusion. The above results obtained by statistical TEM approaches provide direct evidence on the contribution of low oxygen vacancy and high Ag-ion concentrations to the relatively inferior performance of H-Ag-HOL electrode in sodium-ion batteries. In addition to the importance on the appropriate concentration of silver ions and oxygen vacancies determining the resistance of hollandite materials, this study suggests that homogeneity of these environments over the nanorods is

significant enough to reduce inhomogeneous structural evolution of electrodes, which hinders the capability of the materials maximized.

In conclusion, we investigated sodiation behaviors of silver hollandite nanorods by statistical approaches of TEM study. Statistical approaches for data processing of HRTEM-FFT patterns and TEM-EELS eliminated the generalization error, one of the most vulnerable points in TEM investigations, and revealed inhomogeneous structural evolution depending on the local concentration of silver ions and oxygen vacancies in nanorods. By direct comparison between $Ag_{1.66}Mn_8O_{16}$ (H-Ag-HOL) and $Ag_{1.22}Mn_8O_{16}$ (L-Ag-HOL), we clearly showed that H-Ag-HOL nanorods, containing more silver ions and less oxygen vacancies than L-Ag-HOL nanorods, undergo phase/structural transformation at the lower sodiation levels. H-Ag-HOL showed lower average Mn oxidation state under the same sodiation levels with L-Ag-HOL and it reached the interplanar spacing of archetypal MnO lattice planes at earlier sodiation, 8 Na ions in Mn_8O_{16} unit cell. Furthermore, we found that the inhomogeneous structural evolution is more severe in H-Ag-HOL, from the *inside* to *among* respective nanorods. A collection of TEM-EELS data showed that the imbalance of sodiation among nanorods tends to increase with higher sodiation levels in H-Ag-HOL. The preferential structural development near the surface observed by HRTEM analysis confirmed the significant influence of oxygen vacancies on facile sodium-ion diffusion. By precisely comparing two silver hollandite materials, this study directly shows how silver ions and oxygen vacancies influence the sodium-ion diffusion in the tunnel-structured material, which provides insight into future design of electrode materials with improved electrochemical performance.

Acknowledgements

The electron microscopy work reported here was supported by the U.S. Department of Energy, Office of Basic Energy Sciences, Division of Materials Science and Engineering, under Contract No. DE-SC0012704 and the Center for Mesoscale Transport Properties, an Energy Frontier Research Center supported by the U.S. DOE under award DE-SC0012673. EST acknowledges the generous support of William and Jane Knapp.

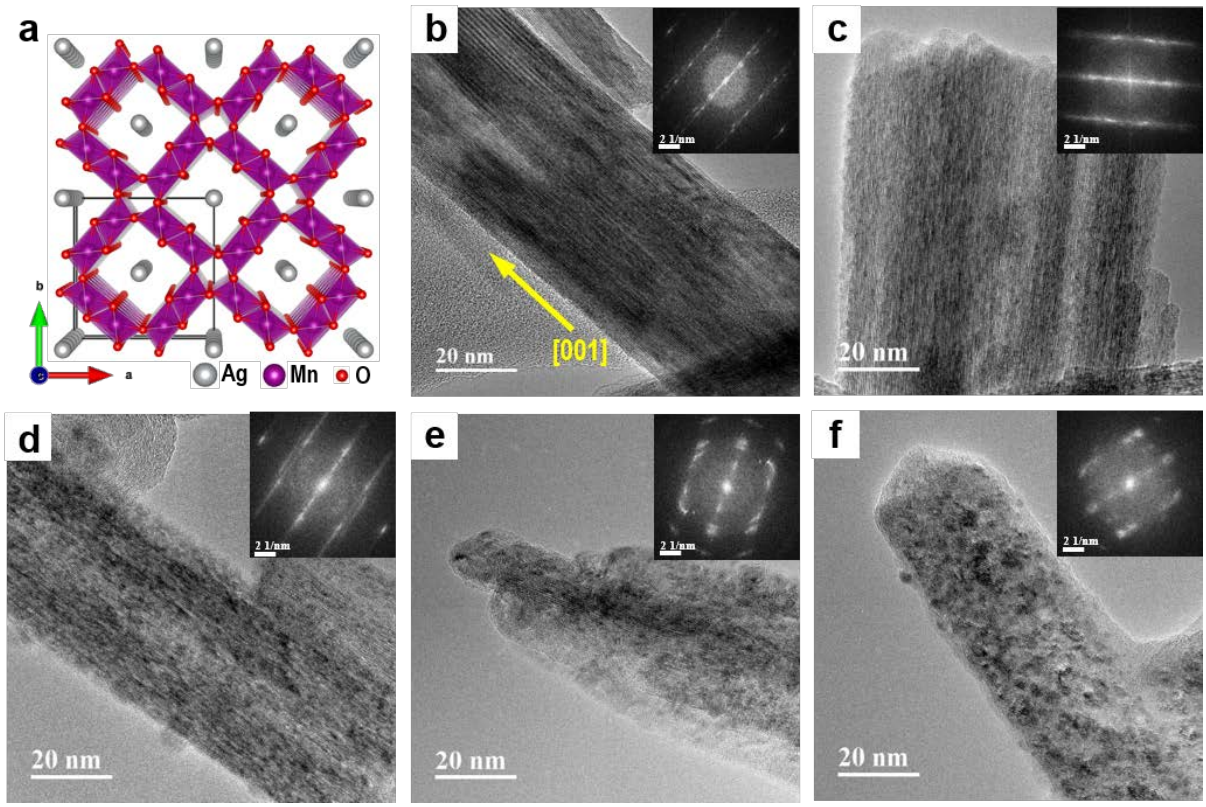

Figure 1. (a) Atomic structural model of an ideal hollandite-structured $Ag_2Mn_8O_{16}$ nanorod at end-on view. (b–f) High-resolution TEM (HRTEM) images showing overall structural changes of $Ag_{1.66}Mn_8O_{16}$ (H-Ag-HOL) nanorods under different sodiation levels. Each image shows sodiated nanorods with (b) 0 (pristine), (c) 2, (d) 4, (e) 6, and (f) 8 Na ions per unit structure, $Ag_{1.66}Mn_8O_{16}$. Fast Fourier transformed (FFT) patterns of the HRTEM images are shown as insets.

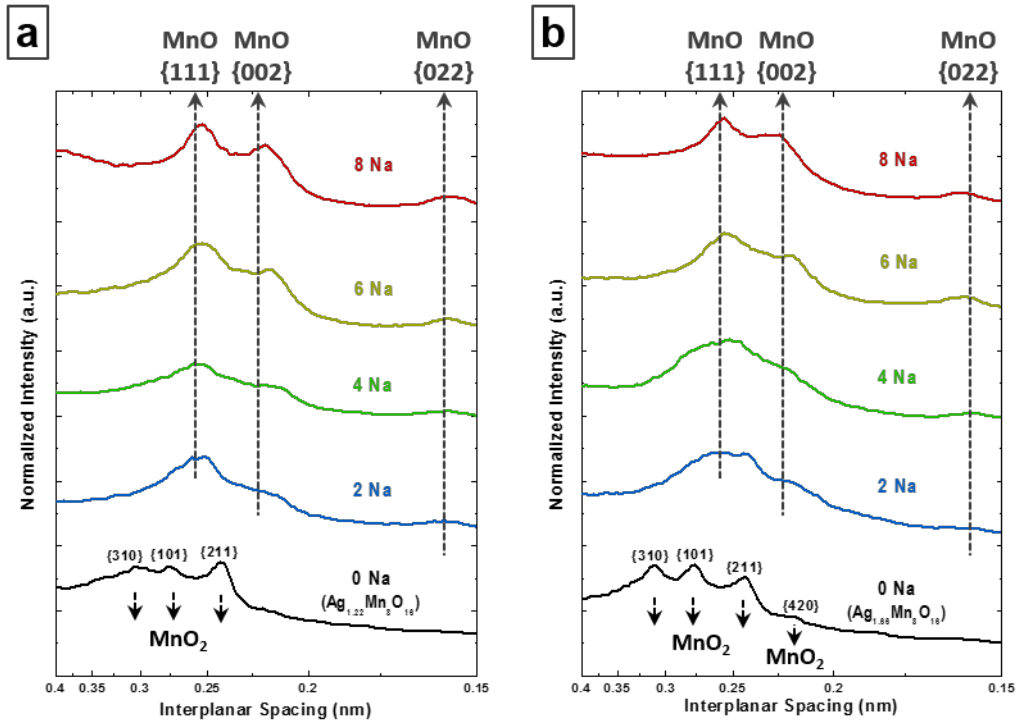

Figure 2. Averaged radial intensity profiles of FFT patterns from HRTEM images of sodiated (a) $Ag_{1.22}Mn_8O_{16}$ (L-Ag-HOL) and (b) $Ag_{1.66}Mn_8O_{16}$ (H-Ag-HOL) nanorods. Sodiation levels are indicated at each curve. Each curve is the sum of normalized radial intensity profiles from over 15 different HRTEM-FFT patterns. Lattice planes corresponding to representative peaks in the curves are indicated on the plot.

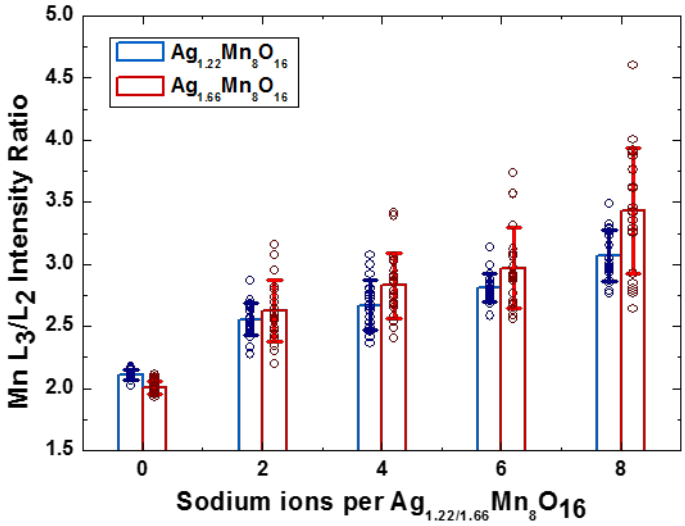

Figure 3. Comparison of TEM-EELS manganese L_3/L_2-edge intensity ratios depending on sodiation levels in $Ag_{1.22}Mn_8O_{16}$ and $Ag_{1.66}Mn_8O_{16}$. TEM-EELS data was taken from over 20 different regions per each sample and each region contains several nanowires. All Mn L_3/L_2-edge intensity ratio values from TEM-EELS data are drawn with open circles at corresponding sodiation levels. The average and standard deviation of Mn L_3/L_2-edge intensity ratios from each sample are plotted with a column and an error bar. The representative experimental TEM-EEL spectra are shown in Figure S3.

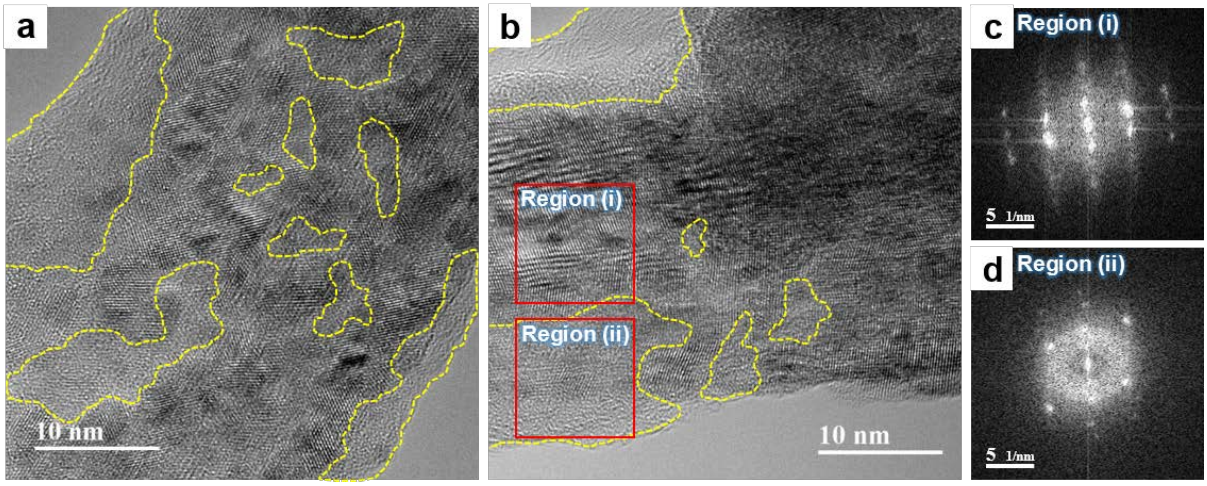

Figure 4. (a, b) Representative HRTEM images and (c, d) FFT patterns showing imbalance of structural evolution between surface and core of a single $Na_8Ag_{1.66}Mn_8O_{16}$ nanorod. (a, b) Yellow closed curves indicate amorphized areas that lost tunnel structural feature.

(c, d) FFT patterns obtained from regions '(i)' and '(ii)' marked in (b).

1. Slater, M. D.; Kim, D.; Lee, E.; Johnson, C. S., Sodium-Ion Batteries. *Adv Funct Mater* **2013,** *23* (8), 947-958.
2. Sun, J.; Lee, H. W.; Pasta, M.; Yuan, H. T.; Zheng, G. Y.; Sun, Y. M.; Li, Y. Z.; Cui, Y., A phosphorene-graphene hybrid material as a high-capacity anode for sodium-ion batteries. *Nat. Nanotechnol.* **2015,** *10* (11), 980-U184.
3. Kundu, D.; Talaie, E.; Duffort, V.; Nazar, L. F., The Emerging Chemistry of Sodium Ion Batteries for Electrochemical Energy Storage. *Angew. Chem. Int. Edit.* **2015,** *54* (11), 3431-3448.
4. Tompsett, D. A.; Islam, M. S., Electrochemistry of Hollandite alpha-MnO2: Li-Ion and Na-Ion Insertion and Li2O Incorporation. *Chem. Mater.* **2013,** *25* (12), 2515-2526.
5. Huang, J. P.; Payraz, A. S.; Lee, S. Y.; Wu, L. J.; Zhu, Y. M.; Marschilok, A. C.; Takeuchi, K. J.; Takeuchi, E. S., Silver-Containing alpha-MnO2 Nanorods: Electrochemistry in Na-Based Battery Systems. *Acs Appl. Mater. Inter.* **2017,** *9* (5), 4333-4342.
6. Zhang, R. G.; Yu, X. Q.; Nam, K. W.; Ling, C.; Arthur, T. S.; Song, W.; Knapp, A. M.; Ehrlich, S. N.; Yang, X. Q.; Matsui, M., alpha-MnO2 as a cathode material for rechargeable Mg batteries. *Electrochem Commun* **2012,** *23*, 110-113.
7. Xu, C. J.; Li, B. H.; Du, H. D.; Kang, F. Y., Energetic Zinc Ion Chemistry: The Rechargeable Zinc Ion Battery. *Angew. Chem. Int. Edit.* **2012,** *51* (4), 933-935.
8. Huang, J. P.; Hu, X. B.; Brady, A. B.; Wu, L. J.; Zhu, Y. M.; Takeuchi, E. S.; Marschilok, A. C.; Takeuchi, K. J., Unveiling the Structural Evolution of Ag1.2Mn8O16 under Coulombically Controlled (De)Lithiation. *Chem. Mater.* **2018,** *30* (2), 366-375.
9. Yang, Z. Z.; Ford, D. C.; Park, J. S.; Ren, Y.; Kim, S.; Kim, H.; Fister, T. T.; Chan, M. K. Y.; Thackeray, M. M., Probing the Release and Uptake of Water in alpha-MnO2 center dot xH(2)O. *Chem. Mater.* **2017,** *29* (4), 1507-1517.
10. Johnson, C. S., Development and utility of manganese oxides as cathodes in lithium batteries. *J. Power Sources* **2007,** *165* (2), 559-565.
11. Yuan, Y. F.; Nie, A. M.; Odegard, G. M.; Xu, R.; Zhou, D. H.; Santhanagopalan, S.; He, K.; Asayesh-Ardakani, H.; Meng, D. D.; Klie, R. F.; Johnson, C.; Lu, J.; Shahbazian-Yassar, R., Asynchronous Crystal Cell Expansion during Lithiation of K+-Stabilized alpha-MnO2. *Nano Lett.* **2015,** *15* (5), 2998-3007.
12. Poyraz, A. S.; Huang, J. P.; Cheng, S. B.; Wu, L. J.; Tong, X.; Zhu, Y. M.; Marschilok, A. C.; Takeuchi, K. J.; Takeuchi, E. S., Tunnel Structured alpha-MnO2 with Different Tunnel Cations (H+, K+, Ag+) as Cathode Materials in Rechargeable Lithium Batteries: The Role of Tunnel Cation on Electrochemistry. *J. Electrochem. Soc.* **2017,** *164* (9), A1983-A1990.
13. Smith, P. F.; Brady, A. B.; Lee, S. Y.; Bruck, A. M.; Dooryhee, E.; Wu, L. J.; Zhu, Y. M.; Takeuchi, K. J.; Takeuchi, E. S.; Marschilok, A. C., Deliberately Designed Atomic-Level Silver-Containing Interface Results in Improved Rate Capability and Utilization of Silver Hollandite for Lithium-Ion Storage. *Acs Appl. Mater. Inter.* **2018,** *10* (1), 400-407.
14. Wu, L. J.; Xu, F.; Zhu, Y. M.; Brady, A. B.; Huang, J. P.; Durham, J. L.; Dooryhee, E.; Marschilok, A. C.; Takeuchi, E. S.; Takeuchi, K. J., Structural Defects of Silver Hollandite, AgxMn8Oy, Nanorods: Dramatic Impact on Electrochemistry. *Acs Nano* **2015,** *9* (8), 8430-8439.
15. Paxton, W. A.; Zhong, Z.; Tsakalakos, T., Tracking inhomogeneity in high-capacity lithium iron phosphate batteries. *J. Power Sources* **2015,** *275*, 429-434.
16. Sasaki, T.; Villevieille, C.; Takeuchi, Y.; Novak, P., Understanding Inhomogeneous Reactions in Li-Ion Batteries: Operando Synchrotron X-Ray Diffraction on Two-Layer Electrodes. *Adv Sci* **2015,** *2* (7).
17. Lee, S. Y.; Wu, L. J.; Poyraz, A. S.; Huang, J. P.; Marschilok, A. C.; Takeuchi, K. J.; Takeuchi, E. S.; Kim, M.; Zhu, Y. M., Lithiation Mechanism of Tunnel-Structured MnO2 Electrode Investigated by In Situ Transmission Electron Microscopy. *Adv. Mater.* **2017,** *29* (43).

18. Pearson, D. H.; Ahn, C. C.; Fultz, B., White Lines and D-Electron Occupancies for the 3d and 4d Transition-Metals. *Phys. Rev. B* **1993,** *47* (14), 8471-8478.
19. Rask, J. H.; Miner, B. A.; Buseck, P. R., Determination of Manganese Oxidation-States in Solids by Electron Energy-Loss Spectroscopy. *Ultramicroscopy* **1987,** *21* (4), 321-326.
20. Kurata, H.; Colliex, C., Electron-Energy-Loss Core-Edge Structures in Manganese Oxides. *Phys. Rev. B* **1993,** *48* (4), 2102-2108.
21. Garvie, L. A. J.; Craven, A. J., High-Resolution Parallel Electron-Energy-Loss Spectroscopy of Mn L(2,3)-Edges in Inorganic Manganese Compounds. *Phys. Chem. Miner.* **1994,** *21* (4), 191-206.